Carbohydrate Polymers 121 (2015) 428–435

Contents lists available at ScienceDirect

Carbohydrate Polymers

journal homepage: www.elsevier.com/locate/carbpol

Layer-by-layer immobilization of quaternized carboxymethyl chitosan/organic rectorite and alginate onto nanofibrous mats and their antibacterial application

Linbin Jiang[a,b], Yuan Lu[a,b], Xingyun Liu[a], Hu Tu[a], Jianwei Zhang[b], Xiaowen Shi[b], Hongbing Deng[b,*], Yumin Du[b]

[a] School of Chemistry and Chemical Engineering, Guangxi Key Laboratory of Petrochemical Resource Processing and Process Intensification Technology, Guangxi University, Nanning 530004, China
[b] School of Resource and Environmental Science, Wuhan University, Wuhan 430079, China

ARTICLE INFO

Article history:
Received 18 October 2014
Received in revised form
23 December 2014
Accepted 25 December 2014
Available online 5 January 2015

Keywords:
Quaternized carboxymethyl chitosan
Organic rectorite
Sodium alginate
Layer-by-layer
Antibacterial activity

ABSTRACT

Quaternized carboxymethyl chitosan (QCM-chitosan) and organic rectorite (OREC) immobilized nanofibrous mats are fabricated via layer-by-layer (LBL) technique in a self-assembly manner. The negatively charged cellulose nanofibrous mats hydrolyzed from electrospun cellulose acetate (CEL) mats are alternately modified with the positively charged QCM-chitosan and OREC intercalated composites and the negatively charged sodium alginate (ALG) via LBL technique. The morphology and antibacterial activity of the resultant mats are studied by changing the number of deposition bilayers, the compositions of dipping solutions and outermost layer. X-ray photoelectron spectroscopy results imply that QCM-chitosan and OREC are coated on cellulose mats. Besides, wide angle X-ray diffraction and small angle X-ray diffraction are applied to investigate the crystalline of the composite mats and the interlayer distance of OREC, respectively. The antibacterial activity of the mats increases with the incorporation of OREC into LBL films.

1. Introduction

Electrostatic layer-by-layer (LBL) self-assembly technique, which is firstly reported by Decher (1997), is an efficient method to form multilayer ultra-thin films. It involves alternating adsorption of oppositely charged polyelectrolytes, particles, and ions on solid substrates (Lee, Kim, Chen, Shao-Horn, & Hammond, 2008; Song et al., 2013; Yang, Yang, Yang, Shen, & Yu, 2006). Natural biopolymers can be deposited on the surface of nanofibers to form composite materials via LBL coating process to endow a broad range of applications, including electrochromic devices (Sheng, Bai, Sun, Li, & Shi, 2011), fuel cells (Sun, Zhao, Yang, Song, & Xue, 2010), and electrochemical field (Li et al., 2011). Encouraged by our progress (Deng, Wang, et al., 2011), the cellulose mats with negatively charged fiber surface, which have low fiber density and good water insolubility, are considered as an ideal template for LBL deposition. It is difficult to obtain the cellulose mats via electrospinning technique. However, the template cellulose mats could be hydrolyzed from the electrospun cellulose acetate (CEL) mats in alkaline solution. Therefore, as the LBL template, the cellulose mats which are obtained by alkaline hydrolysis of CEL mats become popular.

CEL possesses good mechanical properties and relatively low cost. It is not only naturally abundant, but also widely applied in membranes for forward osmosis (Su, Yang, Teo, & Chung, 2010), chiral separation (Sueyoshi, Fukushima, & Yoshikawa, 2010) and water treatment (Tian et al., 2011). Additionally, CEL is easy to be electrospun into nanofibrous mats. The surface of cellulose mats can be modified by depositing other materials with LBL technique to obtain additional properties, such as antimicrobial activity.

In this study, alginate (ALG) and quaternized carboxymethyl chitosan (QCM-chitosan) were used as assembly objects for polyelectrolyte LBL assembling based on their electrical properties (Liu et al., 2012). ALG is a biodegradable linear polysaccharide made of (1 → 4) linked β-D-ManA and α-L-GulA units in varying proportions (Wang et al., 2014). ALG possesses properties of non-toxicity, low cost and hydrophilicity, and it is negatively charged from the carboxylate groups (Shalumon et al., 2011). Chitosan is one of the most abundant cationic polysaccharides with β-1,4-linked N-acetyl-D-glucosamine and D-glucosamine unit (Anitha et al., 2014; Pereda, Ponce, Marcovich, Ruseckaite, & Martucci, 2011), which possesses non-toxicity, biodegradability, and a broad antibacterial

* Corresponding author. Tel.: +86 27 68778501; fax: +86 27 68778501.
E-mail addresses: hbdeng@whu.edu.cn, alphabeita@yahoo.com (H. Deng).

http://dx.doi.org/10.1016/j.carbpol.2014.12.069
0144-8617/

spectrum (Wang, Du, Luo, Lin, & Kennedy, 2007) (Sun, Du, Fan, Chen, & Yang, 2006). However, chitosan only shows the antimicrobial activity in acidic medium due to its poor solubility in neutral aqueous solution. In order to improve the solubility of chitosan and exploit its antimicrobial activity and biochemical significance, amphoteric derivatives are synthesized, such as N-carboxymethyl chitosan, methyl pyrrolidinone chitosan and N-carboxybutyl chitosan (Muzzarelli et al., 1990; Muzzarelli, 1988; Muzzarelli, Ilari, & Tomasetti, 1993; Muzzarelli, Tanfani, Emanuelli, & Mariotti, 1982). QCM-chitosan is a novel promising amphoteric polymer which is obtained by introducing carboxymethyl group and quaternary ammonium salt on chitosan (Ling, Luo, Luo, Wang, & Sun, 2013). The studies have showed many of its applications in antioxidant (Liu et al., 2009), drug encapsulation (Liang et al., 2008) and antibacterial activity (Sun et al., 2006). Interestingly, it has been reported that the antimicrobial activity is obviously enhanced when the chains of the QCM-chitosan is intercalated into the interlayer of organic rectorite (OREC) (Deng et al., 2012). It has also proved that the chitosan-OREC intercalated composites have better antibacterial activity than chitosan itself because OREC could absorb more bacteria and inhibit its growth (Wang et al., 2006).

OREC is modified by cation exchange from REC. OREC is a kind of layered silicate, which has larger interlayer distance, thicker layer and larger aspect ratio than REC or montmorillonite (Deng et al., 2012). It has many properties, including long expectancy of life, high resistance to heat and weak activity of inhibiting mold. In our previous report (Deng et al., 2012), the inhibiting effects of other antimicrobial reagents are remarkably enhanced by the addition of OREC. The positive potential and the enlarged interlayer distance of OREC exert the synergetic antimicrobial effect. As mentioned above, we speculate that the (QCM-chitosan/OREC)/ALG composite multilayers possess enhanced antimicrobial activity in water solution.

In the study, we developed a straightforward method for the fabrication of the nanofibrous mats containing OREC for bacterial inhibition via LBL self-assembling of QCM-chitosan and ALG. The cellulose template was obtained via hydrolyzing the electrospun CEL mats in alkaline solution. The Field Emission Scanning Electron Microscope (FE-SEM) was applied to investigate the morphology. The composition of the multilayer was investigated by Fourier transform infrared spectra (FT-IR) and X-ray photoelectron spectroscope (XPS). The Small angle X-ray diffraction (SAXRD) and Wide angle X-ray diffraction (WAXRD) were employed to study the layered structure of OREC and the crystallization of the mats. Finally the bacterial inhibition experiments were performed to examine the antimicrobial properties of the resultant samples.

2. Materials and methods

2.1. Materials

Cellulose acetate (CEL, $M_n = 3 \times 10^4$) was obtained from Sigma Aldrich Chemical Reagent Co., USA. Calcium rectorite (Ca^{2+}-REC) was supplied by Hubei Mingliu Co., China. Chitosan ($M_w = 2.1 \times 10^5$ Da, DD = 92%) was purchased from Yuhuan Ocean Biochemical Co., China. Sodium alginate (ALG, $M_w = 398.31$) and sodium dodecylsulfonate (SDS) was provided by Aladdin Chemical Reagent Co., China. The 2,3-epoxypropyl trimethylammonium chloride was obtained from Adamas Reagent Co. Ltd., China. Acetone, N,N-dimethylacetamide (DMAc), acetic acid, sodium hydroxide, hydrogen chloride, and sodium chloride were supplied by Aladdin Chemical Reagent Co., China. Chloroacetic acid was provided by Xi Ya Reagent Co., China. *Escherichia coli* and *Staphylococcus aureus* were obtained from State Key Laboratory of Agricultural Microbiology of Huazhong Agricultural University (Wuhan, China). Nutrient agar and nutrient broth were supplied by Qingdao Rishui Biological Technology Co. (Qingdao, China). Other chemicals were of analytical grade. And aqueous solutions were prepared using deionized water with a resistance of 18.2 MΩ cm.

2.2. Preparation of OREC

The OREC was synthesized by cation exchange reactions between REC and SDS. In brief, the REC was dispersed in deionized water to obtain the suspension with vigorous stirring for 72 h, then added SDS slowly into the obtained suspension at 90 °C with 5 h stirring. Additionally, the resultant sample was washed several times with deionized water and filtered to remove excessive SDS. Finally the product was dried at 90 °C to obtain OREC.

2.3. Preparation of quaternized carboxymethyl chitosan (QCM-chitosan)

QCM-chitosan was prepared according to the previous report (Wang et al., 2010). Five grams of chitosan was alkalified by 6 ml of 50% NaOH solution (w/w) and then frozen for 24 h at −20 °C. After 24 h, the frozen alkali chitosan was transferred to three-necked flask. Subsequently, 100 ml of isopropyl alcohol and 6 g of chloroacetic acid were added into frozen alkali chitosan in the three-necked flask. The mixture was kept under stirring at room temperature for 2 h. After that the temperature was elevated to 60 °C, and the mixture was continuously stirred for another 3 h. After 3 h, the mixture was cooled to room temperature and filtered. The residue was dissolved in 250 ml water. The pH value of obtained solution was adjusted to 7.0 with dilute hydrochloric acid solution. Then the solution was dialyzed in deionized water at 25 °C for 5 days followed by rotary evaporation at 65 °C for 90 min, and then lyophilized to obtain carboxymethyl chitosan (CM-chitosan). Three grams of CM-chitosan and 20 ml of water were transferred to a three-necked flask under stirring at 80 °C, then 100 ml of 2,3-epoxypropyl trimethylammonium chloride solution was added into the above mixture solution, and the reaction continued for 8 h. Finally the solution was dialyzed in deionized water at 25 °C for 5 days and lyophilized to obtain the spongy solid QCM-chitosan.

2.4. Preparation of template cellulose nanofibrous mats

Cellulose mats were fabricated based on our previous report (Huang et al., 2012). Sixteen percent of CEL solution was prepared by adding CEL powder into the mixed solution of acetone and DMAc (2:1 in wt/wt). The distance of tip-to-collector, applied voltage and delivery speed of solutions was 20 cm, 16 kV and 1 ml/h, respectively. The ambient temperature and relative humidity were kept at 25 °C and 45%, respectively. Then the as-prepared mats were dried in vacuum at 80 °C for 24 h in order to remove trace solvents. Finally the cellulose nanofibrous mats were obtained by hydrolysis of CEL mats in 0.05 M of NaOH solution at room temperature for 7 days.

2.5. Preparation of LBL structured nanofibrous mats

ALG, QCM-chitosan and QCM-chitosan/OREC solution were prepared as follows. To obtain 1 mg/ml of ALG solution and 1 mg/ml of QCM-chitosan solution, ALG powder and QCM-chitosan powder were dissolved, respectively, in the water under continuous stirring for 4 h at room temperature. The QCM-chitosan/OREC (the mass ratio of a QCM-chitosan and OREC was 6:1) solution with a concentration of 1 mg/ml were fabricated by dropwise adding the QCM-chitosan solution into OREC suspension under stirring for 12 h. The pH values of QCM-chitosan, QCM-chitosan/OREC and ALG solutions were adjusted to 5, 5 and 4, correspondingly. At last, the

ionic strength of solutions was adjusted by adding NaCl solution to a final concentration of 0.1 M.

The LBL structured nanofibrous mats were obtained according Scheme 1. The as-prepared cellulose mats were immersed into QCM-chitosan or QCM-chitosan/OREC solution for 20 min and then the mats were rinsed with NaCl solution for three times. Next, the mats were immersed into ALG solution for another 20 min and then performed the same rinsing steps. The adsorption and rinsing steps were repeated until the desired number of deposition bilayers obtained. $[(\text{QCM-chitosan/OREC})/\text{ALG}]_n$ was used as formula to label the LBL structured mats, where n was the number of the (QCM-chitosan/OREC)/ALG bilayers. When n was 5.5 or 10.5, the outermost layer was QCM-chitosan/OREC. When n was 5 or 10, the outermost was ALG. All the prepared samples were dried under vacuum at 80 °C for 24 h before characterizations.

2.6. Characterizations

ζ-Potential analysis was performed by the Nano-25 zetasizer (Malven, England). Fourier transform infrared (FT-IR) spectra were recorded by the Nicolet 170-SX (Thermo Nicolet Ltd., USA). The surface morphology of nanofibrous mats before and after modification was investigated by field emission scanning electron microscopy (FE-SEM, S-4800, FEI Ltd., Japan). The element composition was analyzed by X-ray photoelectron spectroscopy (XPS) (Kratos, UK). The X-ray diffraction was carried out by the diffractometer type D/max-Ra (Rigaku Co., Japan) with Cu target and $K\alpha$ radiation ($\lambda = 0.154$ nm). The scan speed and scope of the small angle X-ray diffraction (SAXRD) were 1–6° and 1° min^{-1}, and those of the wide angle X-ray diffraction (WAXRD) were 5–60° and 5° min^{-1}, respectively.

2.7. Antibacterial assay

The antimicrobial activity of LBL structured nanofibrous mats against Gram-negative bacteria *E. coli* and Gram-positive bacteria *S. aureus* was investigated by inhibition zone method. The nanofibrous mats were cut into disks with a diameter of 6 mm and then sterilized with an ultraviolet radiation lamp for 30 min. The diluted levitation bacterial (50 μL) with concentration of $5–10 \times 10^5$ CFU/ml was added into the agar culture medium uniformly. Next, the mats disks were tiled to cling to the surface of the agar medium and then incubated at 37 °C for 12 h. The bacterial inhibition zones were measured with a tolerance of 1 mm. Each sample was repeated three times.

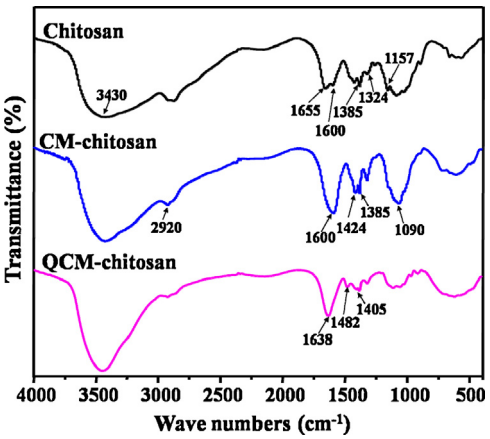

Fig. 1. The FT-IR spectra of chitosan, CM-chitosan and QCM-chitosan.

3. Results and discussion

3.1. FT-IR spectra analysis

Fig. 1 presents the FT-IR spectra of chitosan, CM-chitosan and QCM-chitosan. In the spectrum of chitosan, the characteristic peaks at 1655 and 1600 cm^{-1} were assigned to the C=O stretching of the secondary amide and $-NH_2$ bending of the primary amine (Deng et al., 2012). Besides, the peaks at 3430, 2920, and 1385 cm^{-1} stood for —OH stretching vibration, $-CH_2-$ asymmetrical stretching vibration and vibration bends. Peaks around 1030 and 1090 cm^{-1} attributed to primary and secondary hydroxyl groups vibration bends, respectively (Deng et al., 2013). In the spectrum of CM-chitosan, the peaks of amides I at 1655 cm^{-1} and primary hydroxyl groups at 1030 cm^{-1} disappeared. In addition, the peaks at 2920 and 1424 cm^{-1} were relatively strong, which corresponded to the $-CH_3$ vibration bends, asymmetrical and symmetrical stretching of $-COO^-$ group (Wang et al., 2010). In the spectrum of QCM-chitosan, the peaks at 2956 and 1638 cm^{-1} assigned to $-CH_3$ stretching vibration and $-NH_2$ vibration bends. More importantly, the new peak at 1482 cm^{-1} appeared in the spectrum of QCM-chitosan but not in the spectra of chitosan and CM-chitosan, which attributed to the methyl groups of the ammonium (Wang et al., 2010). It was demonstrated that the 2,3-epoxypropyl trimethylammonium chloride was reacted with CM-chitosan to synthesize the QCM-chitosan.

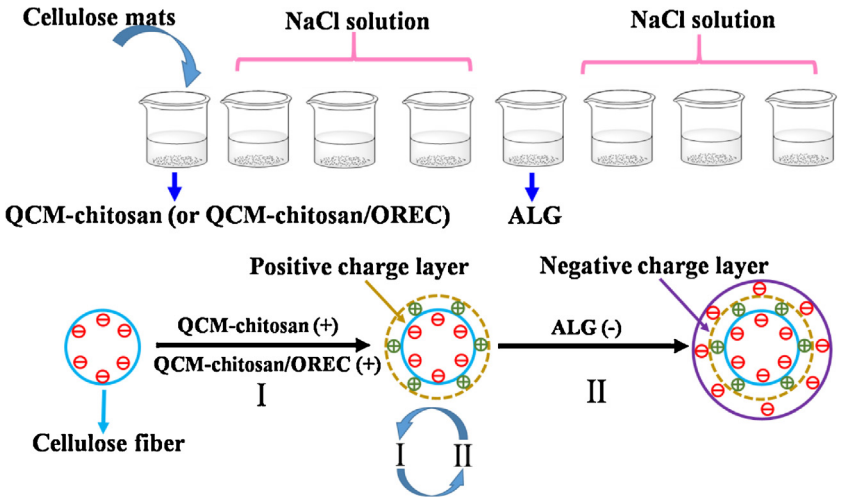

Scheme 1. Schematic diagram illustrating the LBL modification on the mats.

Table 1
ζ-Potential (mV) of OREC, QCM-chitosan, QCM-chitosan/OREC composites, ALG, and cellulose mats.

Samples	OREC	QCM-chitosan	QCM-chitosan/OREC	ALG	Cellulose
ζ-Potential (mV)	+27.9	+30.5	+32.8	−68.1	−21.2

3.2. ζ-Potential analysis

The ζ-potential values of assembly materials and template influence the effect of LBL modification. Table 1 shows the ζ-potential values of coating materials and cellulose template. It could be observed that the OREC, QCM-chitosan and QCM-chitosan/OREC composites were positively charged and the ζ-potential values were +27.9, +30.5 and +32.8 mV, respectively. The ζ-potential value of QCM-chitosan/OREC composites was slightly higher than that of OREC and QCM-chitosan. On the other side, the ALG and cellulose nanofibrous mats were negatively charged and the ζ-potential values were −68.1 and −21.2 mV, respectively. Hence, the positively charged QCM-chitosan (or QCM-chitosan/OREC composites) and negatively charged ALG could be alternately assembled on the

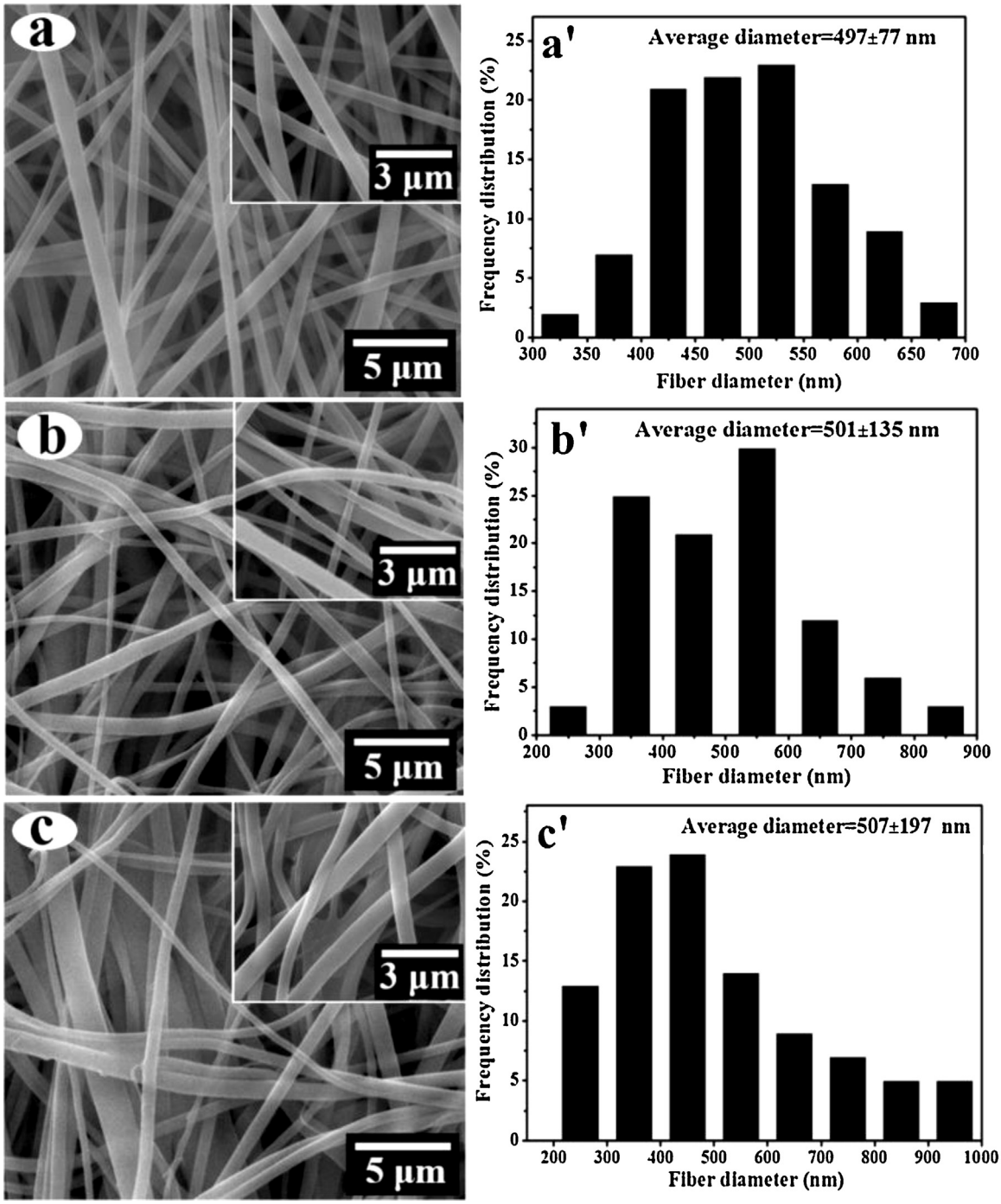

Fig. 2. FE-SEM images of (a) cellulose mats, (b) (QCM-chitosan/ALG)$_5$ and (c) (QCM-chitosan/ALG)$_{10.5}$. Images (a′–c′) show the fiber diameter distributions of (a–c), respectively.

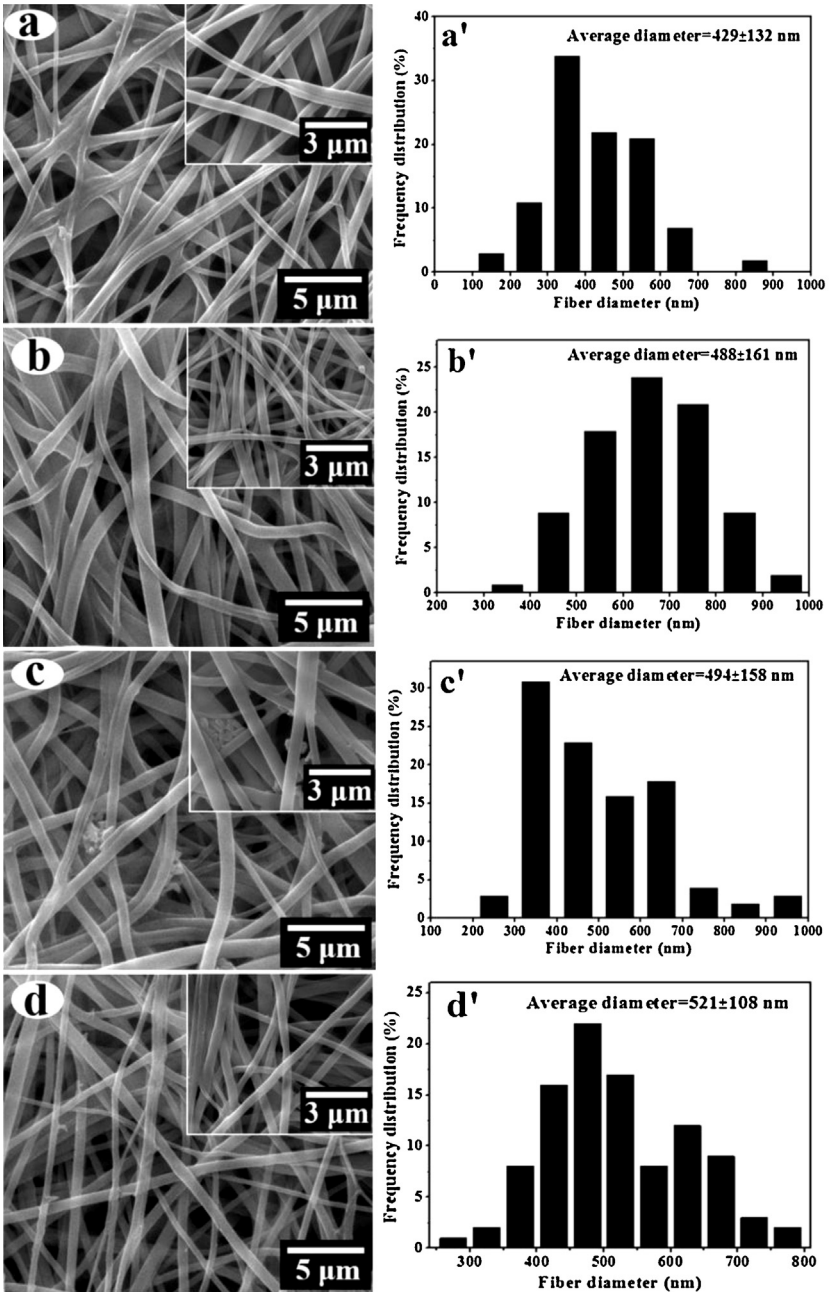

Fig. 3. FE-SEM images of (a) $[(QCM\text{-}chitosan/OREC)/ALG]_5$, (b) $[(QCM\text{-}chitosan/OREC)/ALG]_{5.5}$, (c) $[(QCM\text{-}chitosan/OREC)/ALG]_{10}$ and (d) $[(QCM\text{-}chitosan/OREC)/ALG]_{10.5}$. Images (a′–d′) show the fiber diameter distributions of (a–d), respectively.

surface of negatively charged cellulose mats via electrostatic interactions.

3.3. Morphology of the nanofibrous mats

Fig. 2 displays the FE-SEM images of the nanofibrous mats and their relatively fiber diameter distributions. The cellulose mats showed straight and cylindrical fibers with the average diameter of 497 ± 77 nm (Fig. 2a). After coating QCM-chitosan and ALG, some junctions were observed among the fibers due to the remained solvent evaporation, resulting in the splitting of the polymer films (Fig. 2b and c). It was not surprising that some fibers were bundled parallelly and merged together with adjacent fibers along the fiber axis. It might because the positively charged QCM-chitosan and negatively charged ALG were assembled on the surface of negatively charged fibers, therefore the adjacent fibers were adsorbed through electrostatic interaction. Furthermore, when the number of bilayers was 10.5 (Fig. 2c), the parallel bundles were more than those in the $(QCM\text{-}chitosan/ALG)_5$. Therefore the above results illustrated that the number of coating bilayers extremely affected the morphology.

Fig. 3 exhibits the FE-SEM images of the nanofibrous mats and their fiber diameter distributions after adding OREC into the coating bilayers. Obviously, all the LBL films coated mats showed 3D structure, continuous dense fibers and lots of parallel bundles. The parallel bundles of $[(QCM\text{-}chitosan/OREC)/ALG]_5$ (Fig. 3a) were more than those of $(QCM\text{-}chitosan/ALG)_5$ (Fig. 2b). The reason might be that the addition of OREC could result in increased charge on the surface of QCM-chitosan/OREC composites, which reinforced the electrostatic interaction among fibers. Besides, some fibers adhered together to forming junctions, which were caused by the solvent incompletely volatilization during electrospinning.

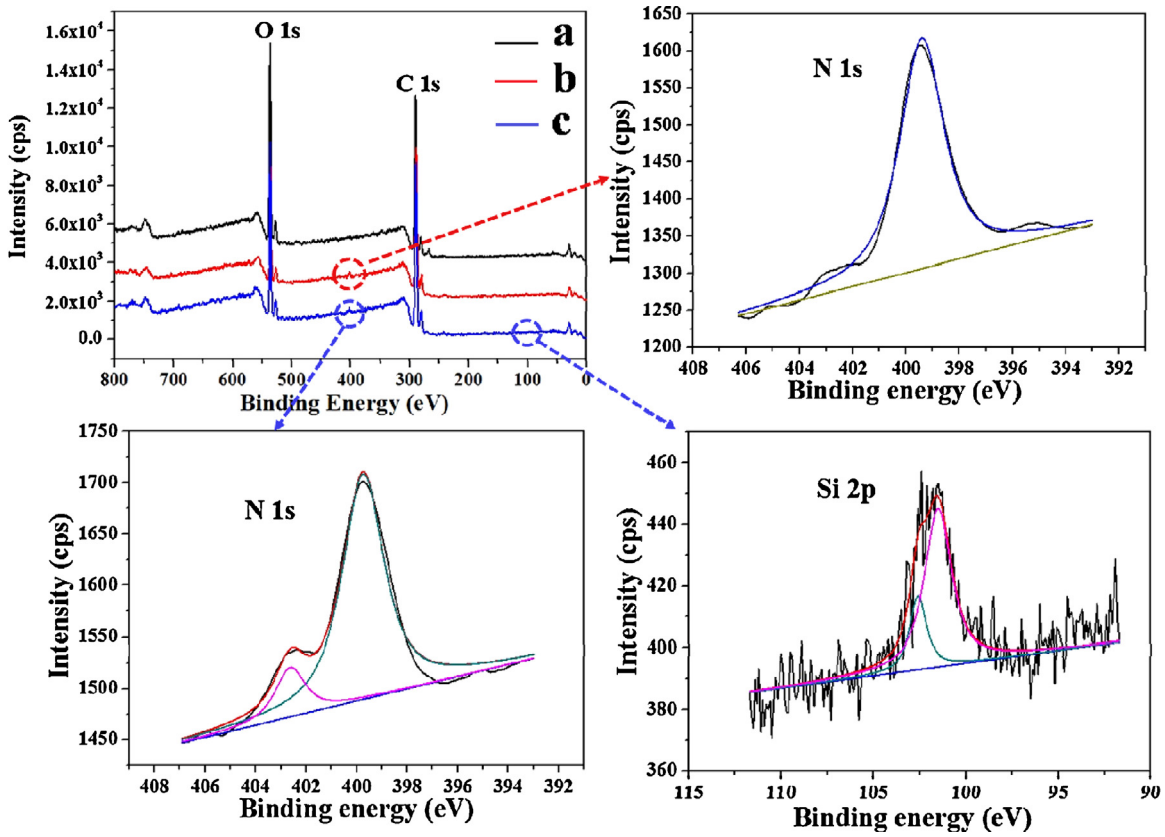

Fig. 4. XPS peak fitting curve of (a) cellulose mats, (b) (QCM-chitosan/ALG)$_{10.5}$ and (c) [(QCM-chitosan/OREC)/ALG]$_{10.5}$, and the narrow scans of N 1s and Si 2p from (b) and (c).

Compared with the smooth surface of the cellulose fibers, the samples (Fig. 3c and d) demonstrated some surface roughness on each fiber by forming some protuberances, which could be regarded as the irregular deposition of LBL films, caused by the inhomogenous dispersion speed of deposition materials on the cellulose mats (Ding, Li, Fujita, & Shiratori, 2006).

3.4. Composition analysis

Fig. 4 illustrates the XPS peak fitting curve of the samples. It could be distinctly observed that the peaks around 290.3 and 536.0 eV were C 1s and O 1s, respectively. Notably, there was a weakly peak of N 1s around 399.0 eV in the XPS curve fitting of (QCM-chitosan/ALG)$_{10.5}$ (Fig. 4b) and [(QCM-chitosan/OREC)/ALG]$_{10.5}$ (Fig. 4c), which confirmed that the QCM-chitosan was deposited on the surface of LBL films coatings. In the XPS narrow scan of (QCM-chitosan/ALG)$_{10.5}$, the N 1s peak around 399.4 eV attributed to the N of $-N(CH_3)_3$ groups. However, in Fig. 4C, the signal of N 1s showed two peaks at 402.6 and 399.5 eV, which belonged to $-N{\equiv}Si_3$ and $-N(CH_3)_3$ groups, respectively (Huang et al., 2014). The result demonstrated that the interaction between OREC and QCM-chitosan molecular was existed in the QCM-chitosan/OREC composites and Si atom was bonded to N atom. The XPS narrow scan of Si element showed two peaks at 101.4 and 102.6 eV, respectively. It can be concluded that OREC was deposited on the surface of [(QCM-chitosan/OREC)/ALG]$_{10.5}$.

3.5. SAXRD and WAXRD patterns

SAXRD was employed to investigate the building of predesigned intercalated architecture in LBL films coated mats, further analyze the interaction between layered silicate and polymer molecular. Fig. 5 presents the SAXRD patterns of OREC, QCM-chitosan/OREC composites and [(QCM-chitosan/OREC)/ALG]$_{10.5}$, and its maximum intensity of peaks was located at $2\theta = 1.92^\circ$, 1.88° and 1.62°, respectively. According to the Bragg's equation $2d \sin\theta = n\lambda$, the corresponding interlayer distances were calculated as 4.60, 4.70 and 5.45 nm, respectively.

In comparison with OREC, the interlayer distance of OREC in the QCM-chitosan/OREC composites increased. The probable reason for this phenomenon was the formation of electrostatic repulsion and hydrogen bond between the surface of OREC and QCM-chitosan molecular (Deng, Li, et al., 2011). The QCM-chitosan (+30.5 eV) and OREC (+27.9 eV) were positively charged and the QCM-chitosan molecular could insert into the interlayer of OREC, so the

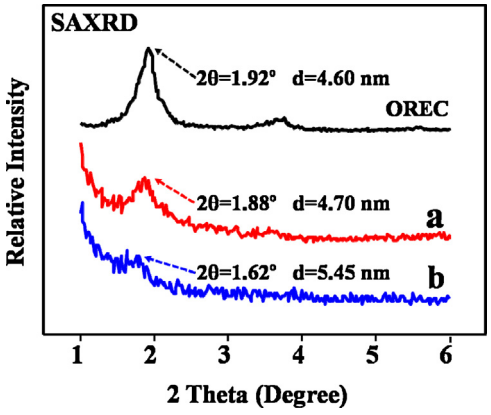

Fig. 5. SAXRD patterns of (a) QCM-chitosan/OREC composites and (b) [(QCM-chitosan/OREC)/ALG]$_{10.5}$.

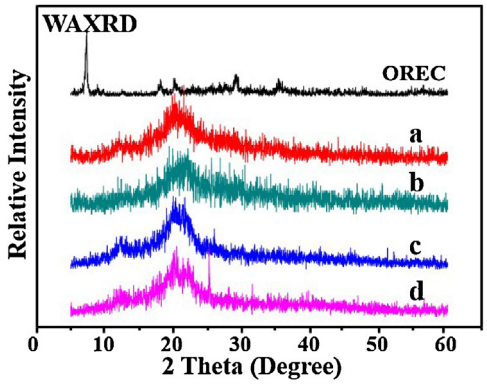

Fig. 6. WAXRD patterns of (a) cellulose, (b) $[(QCM\text{-}chitosan/OREC)/ALG]_5$, (c) $(QCM\text{-}chitosan/ALG)_{10.5}$ and (d) $[(QCM\text{-}chitosan/OREC)/ALG]_{10.5}$.

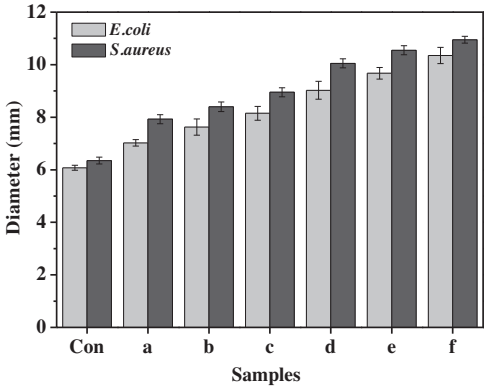

Fig. 7. Antimicrobial activities against *E. coli* and *S. aureus*: (a) $(QCM\text{-}chitosan/ALG)_5$, (b) $[(QCM\text{-}chitosan/OREC)/ALG]_5$, (c) $[(QCM\text{-}chitosan/OREC)/ALG]_{5.5}$, (d) $(QCM\text{-}chitosan/ALG)_{10.5}$, (e) $[(QCM\text{-}chitosan/OREC)/ALG]_{10}$ and (f) $[(QCM\text{-}chitosan/OREC)/ALG]_{10.5}$.

electrostatic repulsion could enlarge the interlayer distance of OREC. In addition, when the number of coating bilayers reached at 10.5, the gallery distance of OREC in the $[(QCM\text{-}chitosan/OREC)/ALG]_{10.5}$ increased in comparison with that of the bulk OREC. Because more QCM-chitosan chains were gradually intercalated into the interlayer of OREC and then the further swelling of QCM-chitosan molecular could enlarge the interlayer distance of OREC.

In order to investigate whether the effect of deposition materials and the number of coating bilayers on the crystalline properties of composite nanofibrous mats, the WAXRD patterns of samples were shown in Fig. 6. In the WAXRD pattern of OREC, there were five characteristic peaks as follows: 7.34°, 18.06°, 21.16°, 29.06° and 35.84°, which was in agreement with our previous report (Li et al., 2013). The two crystalline peaks of cellulose mats (Fig. 6a), $(QCM\text{-}chitosan/ALG)_{10.5}$ (Fig. 6c) and $[(QCM\text{-}chitosan/OREC)/ALG]_{10.5}$ (Fig. 6d) were around 12.08° and 20.82°, respectively. The result demonstrated that the QCM-chitosan and QCM-chitosan/OREC have not affected the crystallization of cellulose mats when the outmost layer of LBL films coated mats was positively charged QCM-chitosan and QCM-chitosan/OREC. Compared with the WAXRD curve of cellulose mats, the crystalline peak of $[(QCM\text{-}chitosan/OREC)/ALG]_5$ mats (Fig. 6b) at 12.08° disappeared and its strong peak was shifted to 22.12°. It indicated that the ALG molecular could influence the crystalline properties of cellulose mats when the outermost layer of LBL films coated mats was negatively charged ALG. In addition, in the WAXRD patterns of $[(QCM\text{-}chitosan/OREC)/ALG]_5$ and $[(QCM\text{-}chitosan/OREC)/ALG]_{10.5}$, the diffraction peaks of OREC could not be observed.

3.6. Antibacterial activity

In order to investigate the antibacterial properties of nanofibrous mats before and after deposition, the antibacterial experiment was carried out and the Gram-negative *E. coli* and Gram-positive *S. aureus* were chosen as the representative microorganisms. Fig. 7 exhibits the results of antibacterial experiment of the uncoated and LBL films coated cellulose mats against *E. coli* and *S. aureus*. It was observed that all the nanofibrous mats before and after modification had the bacterial inhibition activity against *E. coli* and *S. aureus* and the antibacterial ability of LBL films coated mats was better than that of cellulose mats. Here, cellulose mats was covered on the surface of the bacteria colonies and inhibited O_2 and CO_2 contacting with bacteria, therefore the bacteria could be killed. Besides, the antibacterial activity of mats increased with the number of coating bilayers because the QCM-chitosan possessed good antibacterial ability and the content of QCM-chitosan deposited on the surface of LBL films coated mats increased. In addition, antibacterial activity of the uncoated and LBL films coated cellulose mats exhibited lower inhibitory activity against *E. coli* than that of *S. aureus*. Compared Fig. 7b with c, as well as Fig. 7e with f, it could be found that the bacterial inhibition activity of LBL films coated mats with QCM-chitosan/OREC in the outmost layer was higher than that of ALG in the outmost layer. Because the QCM-chitosan molecular had the positively charged amino group which could react with phospholipids and protein resulted in the damage of the cell wall. Hence, the bacterial growth was inhibited by QCM-chitosan/OREC. The other reason was that the lipopolysaccharide layer of Gram-negative *E. coli* was thicker than that of Gram-positive *S. aureus*, which could protect the cell wall to be destroyed by QCM-chitosan or QCM-chitosan/OREC. Compared Fig. 7a with b, as well as Fig. 7d with f, the addition of OREC could enhance the bacterial inhibition activity of LBL films coated cellulose mats, which was consistent with our previously study (Deng, Wang, et al., 2011). The OREC had the role of synergistic antimicrobial after the OREC was modification by cation exchange between REC and SDS.

4. Conclusions

The positively charged QCM-chitosan/OREC composites and the negatively charged ALG were successfully alternatively immobilized onto the surface of the cellulose mats via LBL self-assembly technique. The morphology of LBL films coated cellulose mats was greatly influenced by the deposition conditions. The resultant samples still maintained perfect fiber shape and 3D structure. The XPS scans showed that both OREC and QCM-chitosan were assembled on the surface of the fibers. The SAXRD demonstrated that the interlayer of OREC was intercalated by QCM-chitosan and the interlayer distance of OREC was enlarged by QCM-chitosan chains. The antibacterial activity of nanofibrous mats increased with the number of coating bilayers and the incorporation of OREC into LBL films.

Acknowledgments

This project was funded by the National Natural Science Foundation of China (Nos. 31101365 and 51473125), and partially supported by the Key Project of Natural Science Foundation of Guangxi Province of China (No. 2011GXNSFD018012).

References

Anitha, A., Sowmya, S., Kumar, P., Deepthi, S., Chennazhi, K., Ehrlich, H., et al. (2014). Chitin and chitosan in selected biomedical applications. *Progress in Polymer Science, 39*, 1644–1667.

Decher, G. (1997). Fuzzy nanoassemblies: Toward layered polymeric multicomposites. *Science*, *277*(5330), 1232–1237.
Deng, H., Li, X., Ding, B., Du, Y., Li, G., Yang, J., et al. (2011). Fabrication of polymer/layered silicate intercalated nanofibrous mats and their bacterial inhibition activity. *Carbohydrate Polymers*, *83*(2), 973–978.
Deng, H., Wang, X., Liu, P., Ding, B., Du, Y., Li, G., et al. (2011). Enhanced bacterial inhibition activity of layer-by-layer structured polysaccharide film-coated cellulose nanofibrous mats via addition of layered silicate. *Carbohydrate Polymers*, *83*(1), 239–245.
Deng, H., Lin, P., Xin, S., Huang, R., Li, W., Du, Y., et al. (2012). Quaternized chitosan-layered silicate intercalated composites based nanofibrous mats and their antibacterial activity. *Carbohydrate Polymers*, *89*(2), 307–313.
Deng, H., Lin, P., Li, W., Xin, S., Zhou, X., & Yang, J. (2013). Hydroxypropyl chitosan/organic rectorite-based nanofibrous mats with intercalated structure for bacterial inhibition. *Journal of Biomaterials Science, Polymer Edition*, *24*(4), 485–496.
Ding, B., Li, C., Fujita, S., & Shiratori, S. (2006). Layer-by-layer self-assembled tubular films containing polyoxometalate on electrospun nanofibers. *Colloids and Surfaces A: Physicochemical and Engineering Aspects*, *284*, 257–262.
Huang, W., Xu, H., Xue, Y., Huang, R., Deng, H., & Pan, S. (2012). Layer-by-layer immobilization of lysozyme–chitosan–organic rectorite composites on electrospun nanofibrous mats for pork preservation. *Food Research International*, *48*(2), 784–791.
Huang, R., Zhou, X., Liu, X., Zhang, Q., Jin, H., Shi, G., et al. (2014). Nanofibrous mats layer-by-layer assembled by HTCC/layered silicate composites with in vitro anti-tumor activity against SMMC-7721 cells. *Journal of Biomedical Nanotechnology*, *10*(3), 485–499.
Lee, S. W., Kim, B.-S., Chen, S., Shao-Horn, Y., & Hammond, P. T. (2008). Layer-by-layer assembly of all carbon nanotube ultrathin films for electrochemical applications. *Journal of the American Chemical Society*, *131*(2), 671–679.
Li, Z., Wang, J., Liu, X., Liu, S., Ou, J., & Yang, S. (2011). Electrostatic layer-by-layer self-assembly multilayer films based on graphene and manganese dioxide sheets as novel electrode materials for supercapacitors. *Journal of Materials Chemistry*, *21*(10), 3397–3403.
Li, W., Li, X., Chen, Y., Li, X., Deng, H., Wang, T., et al. (2013). Poly(vinyl alcohol)/sodium alginate/layered silicate based nanofibrous mats for bacterial inhibition. *Carbohydrate Polymers*, *92*(2), 2232–2238.
Liang, X. F., Wang, H. J., Luo, H., Tian, H., Zhang, B. B., Hao, L. J., et al. (2008). Characterization of novel multifunctional cationic polymeric liposomes formed from octadecyl quaternized carboxymethyl chitosan/cholesterol and drug encapsulation. *Langmuir*, *24*(14), 7147–7153.
Ling, Y., Luo, Y., Luo, J., Wang, X., & Sun, R. (2013). Novel antibacterial paper based on quaternized carboxymethyl chitosan/organic montmorillonite/Ag NP nanocomposites. *Industrial Crops and Products*, *51*, 470–479.
Liu, J., Sun, H., Dong, F., Xue, Q., Wang, G., Qin, S., et al. (2009). The influence of the cation of quaternized chitosans on antioxidant activity. *Carbohydrate Polymers*, *78*(3), 439–443.
Liu, X., Chen, X., Li, Y., Wang, X., Peng, X., & Zhu, W. (2012). Preparation of superparamagnetic Fe_3O_4@alginate/chitosan nanospheres for *Candida rugosa* lipase immobilization and utilization of layer-by-layer assembly to enhance the stability of immobilized lipase. *ACS Applied Materials & Interfaces*, *4*(10), 5169–5178.
Muzzarelli, R. A. (1988). Carboxymethylated chitins and chitosans. *Carbohydrate Polymers*, *8*(1), 1–21.
Muzzarelli, R. A., Tanfani, F., Emanuelli, M., & Mariotti, S. (1982). *N*-(carboxymethylidene) chitosans and *N*-(carboxymethyl) chitosans: Novel chelating polyampholytes obtained from chitosan glyoxylate. *Carbohydrate Research*, *107*(2), 199–214.
Muzzarelli, R., Tarsi, R., Filippini, O., Giovanetti, E., Biagini, G., & Varaldo, P. (1990). Antimicrobial properties of N-carboxybutyl chitosan. *Antimicrobial Agents and Chemotherapy*, *34*(10), 2019–2023.
Muzzarelli, R. A., Ilari, P., & Tomasetti, M. (1993). Preparation and characteristic properties of 5-methyl pyrrolidinone chitosan. *Carbohydrate Polymers*, *20*(2), 99–105.
Pereda, M., Ponce, A., Marcovich, N., Ruseckaite, R., & Martucci, J. (2011). Chitosan–gelatin composites and bi-layer films with potential antimicrobial activity. *Food Hydrocolloids*, *25*(5), 1372–1381.
Shalumon, K., Anulekha, K., Nair, S. V., Nair, S., Chennazhi, K., & Jayakumar, R. (2011). Sodium alginate/poly (vinyl alcohol)/nano ZnO composite nanofibers for antibacterial wound dressings. *International Journal of Biological Macromolecules*, *49*(3), 247–254.
Sheng, K., Bai, H., Sun, Y., Li, C., & Shi, G. (2011). Layer-by-layer assembly of graphene/polyaniline multilayer films and their application for electrochromic devices. *Polymer*, *52*(24), 5567–5572.
Song, R., Yan, J., Xu, S., Wang, Y., Ye, T., Chang, J., et al. (2013). Silver ions/ovalbumin films layer-by-layer self-assembled polyacrylonitrile nanofibrous mats and their antibacterial activity. *Colloids and Surfaces B: Biointerfaces*, *108*, 322–328.
Su, J., Yang, Q., Teo, J. F., & Chung, T.-S. (2010). Cellulose acetate nanofiltration hollow fiber membranes for forward osmosis processes. *Journal of Membrane Science*, *355*(1), 36–44.
Sueyoshi, Y., Fukushima, C., & Yoshikawa, M. (2010). Molecularly imprinted nanofiber membranes from cellulose acetate aimed for chiral separation. *Journal of Membrane Science*, *357*(1), 90–97.
Sun, L., Du, Y., Fan, L., Chen, X., & Yang, J. (2006). Preparation, characterization and antimicrobial activity of quaternized carboxymethyl chitosan and application as pulp-cap. *Polymer*, *47*(6), 1796–1804.
Sun, J.-J., Zhao, H.-Z., Yang, Q.-Z., Song, J., & Xue, A. (2010). A novel layer-by-layer self-assembled carbon nanotube-based anode: Preparation, characterization, and application in microbial fuel cell. *Electrochimica Acta*, *55*(9), 3041–3047.
Tian, Y., Wu, M., Liu, R., Li, Y., Wang, D., Tan, J., et al. (2011). Electrospun membrane of cellulose acetate for heavy metal ion adsorption in water treatment. *Carbohydrate Polymers*, *83*(2), 743–748.
Wang, X., Du, Y., Yang, J., Wang, X., Shi, X., & Hu, Y. (2006). Preparation, characterization and antimicrobial activity of chitosan/layered silicate nanocomposites. *Polymer*, *47*(19), 6738–6744.
Wang, X., Du, Y., Luo, J., Lin, B., & Kennedy, J. F. (2007). Chitosan/organic rectorite nanocomposite films: Structure, characteristic and drug delivery behaviour. *Carbohydrate Polymers*, *69*(1), 41–49.
Wang, X., Liu, B., Ren, J., Liu, C., Wang, X., Wu, J., et al. (2010). Preparation and characterization of new quaternized carboxymethyl chitosan/rectorite nanocomposite. *Composites Science and Technology*, *70*(7), 1161–1167.
Wang, Z., Zhang, X., Gu, J., Yang, H., Nie, J., & Ma, G. (2014). Electrodeposition of alginate/chitosan layer-by-layer composite coatings on titanium substrates. *Carbohydrate Polymers*, *103*, 38–45.
Yang, M., Yang, Y., Yang, H., Shen, G., & Yu, R. (2006). Layer-by-layer self-assembled multilayer films of carbon nanotubes and platinum nanoparticles with polyelectrolyte for the fabrication of biosensors. *Biomaterials*, *27*(2), 246–255.